RSC Advances

PAPER

View Article Online
View Journal | View Issue

Cite this: *RSC Adv.*, 2025, **15**, 4149

Synergizing PIERS and photocatalysis effects in a photo-responsive Ag/TiO_2 nanostructure for an ultrasensitive and renewable PI-PC SERS technique†

Quan-Doan Mai, *[a] Dang Thi Hanh Trang,[a] Ta Ngoc Bach,[b] Vo Thi Le Na,[c] Anh-Tuan Pham[c] and Anh-Tuan Le *[ac]

Surface-enhanced Raman spectroscopy (SERS) is a renowned analytical technique for non-invasive molecular identification. Advancements in SERS technology pivot on designing nano-structured substrates to enhance sensitivity and reliability. A key emerging trend involves integrating pre-treatment and post-treatment techniques on these substrates, leveraging advanced nanostructures to bring unique features, such as ultrasensitivity or reusability, to bridge the gap between laboratory and real-world applications of the SERS technique. Despite these advances, the synergistic application of pre- and post-treatment techniques on a single SERS substrate to fully exploit unique physicochemical effects remains underexplored. To address this, we introduce photo-induced-photo-catalytic SERS (PI-PC SERS), a novel technique that synergistically combines photo-induced enhanced Raman scattering (PIERS) and photocatalysis using a single Ag/TiO_2 nanocomposite structure. This method aims to deliver ultrasensitive sensing capabilities and reusability. The PI-PC SERS technique involves pre-irradiating the SERS substrate with UV light to amplify the Raman signal and post-irradiating to remove fouled analytes. Pre-irradiation enhances the SERS signal by several orders of magnitude compared to normal SERS, attributed to the PIERS effect. Consequently, the detection sensitivity for methylene blue (MB) using PI-PC SERS reaches 1.02×10^{-14} M, significantly better than the 3.04×10^{-11} M achieved with normal SERS. Similar enhancements are observed for thiram, with a limit of detection (LOD) of 1.02×10^{-11} M for PI-PC SERS compared to 2.19×10^{-9} M for normal SERS. Additionally, post-irradiation facilitates the removal of analyte molecules *via* photocatalysis, restoring the substrate to its pristine state, as the byproducts – water and CO_2 gas – are easily managed. Our findings demonstrate that PI-PC SERS creates ultrasensitive sensors and ensures substrate cleanliness and longevity. This method shows great promise for ultrasensitive, sustainable, and cost-effective applications in chemical sensing and molecular diagnostics.

Received 29th October 2024
Accepted 31st January 2025

DOI: 10.1039/d4ra07718k

rsc.li/rsc-advances

1. Introduction

Surface-enhanced Raman spectroscopy (SERS) sensors have garnered significant attention due to their distinct advantages over other sensing platforms, such as label-free, non-invasive, and ultrasensitive detection capabilities, extending to the single-molecule level. Light interacting with molecules can produce a Raman signal, while the addition of nanostructures creates a three-body interaction among light, nanostructures, and molecules, generating a SERS signal where the Raman signal is amplified by millions of times.[1–4] Consequently, the design and implementation of nanostructures, known as SERS substrates, are critical for achieving optimal SERS signals while maintaining reliability and experimental feasibility.[5–7] Over the past decades, significant progress has been made in the development of SERS substrates, with a primary focus on the fabrication of nanostructures. These nanostructures range from simple metallic nanoparticles with controllable arrangements to complex core–shell structures and composites of two or three components, known as nanocomposites.[8–16] Such designs have demonstrated exceptional SERS sensing capabilities across a wide range of analytes.[17–19] Recently, the escalating demands for practical SERS applications have necessitated research to

[a]*Phenikaa University Nano Institute (PHENA), Phenikaa University, Hanoi 12116, Vietnam. E-mail: doan.maiquan@phenikaa-uni.edu.vn; tuan.leanh@phenikaa-uni.edu.vn*

[b]*Institute of Materials Science (IMS), Vietnam Academy of Science and Technology, 18 Hoang Quoc Viet, Hanoi 10000, Vietnam*

[c]*Faculty of Materials Science and Engineering (MSE), Phenikaa University, Hanoi 12116, Vietnam*

† Electronic supplementary information (ESI) available. See DOI: https://doi.org/10.1039/d4ra07718k

develop techniques that concurrently ensure high sensitivity, high reliability, and reusability on a single SERS substrate.

Several advanced techniques leveraging external physical interactions with SERS substrates have been introduced, demonstrating exceptional efficiency. These include heat-induced surface-enhanced Raman scattering (HI-SERS), electric-field-induced surface-enhanced Raman scattering (E-SERS), and the more recent photo-induced enhanced Raman scattering (PIERS). Additionally, photocatalytic activity has been effectively incorporated into SERS substrate engineering to develop reusable substrates aimed at sustainability. Huang *et al.* introduced the HI-SERS technique, which significantly enhances the SERS signal of glutathione, a biological molecule, by heating silver colloid substrates before measurements.[20] This method achieved a LOD value of 50 nM for glutathione, compared to 1 μM with normal SERS techniques, showcasing a substantial improvement in sensing efficiency. Almohammed *et al.* demonstrated the E-SERS technique by applying an electric field (10–25 V mm^{-1}) to aligned semiconducting peptide nanotube–graphene oxide composite structures during SERS measurements.[21] This approach enabled nanomolar detection sensitivity for glucose and nucleobases, with up to a tenfold signal enhancement compared to metal-based substrates. The PIERS technique, as demonstrated by Ben-Jaber *et al.*, showed significantly enhanced sensing efficiency over normal SERS.[22] By irradiating metal/semiconductor-structured SERS substrates with UV light before conducting SERS measurements, they observed a substantial increase in the SERS signal of analytes compared to non-irradiated substrates. Wu *et al.* introduced a reusable SERS substrate based on the photocatalytic activity of Au@Cu_2O–Ag nanocomposites.[23] After SERS measurements of the analyte malachite green (MG), the Au@Cu_2O–Ag substrates were irradiated with UV light, effectively decomposing MG molecules *via* photocatalysis. This process rejuvenated the SERS substrates, making them ready for subsequent measurements. This innovation addresses the issue of waste associated with single-use SERS substrates due to residual analytes, providing economic and environmental benefits, and aligning with sustainability goals. These advancements underscore the potential of integrating external physical interactions and photocatalytic activity in SERS substrate design, paving the way for ultra-sensitive, reliable, and sustainable sensing technologies.

The effectiveness of the developed techniques surrounding SERS has been convincingly demonstrated. However, each technique has its limitations. For example, HI-SERS requires substrates to sustain high temperatures during pre-treatment, which limits the use of SERS materials and also restricts its applications due to the effect of temperature on heat-sensitive analytes. The E-SERS technique necessitates the application of a continuous electric field during measurements, as the electric field effect disappears immediately after the voltage is removed. This requirement for complex substrate fabrication poses scalability challenges. The PIERS technique can eliminate the need for continuous irradiation during measurement, significantly simplifying experimental procedures. However, it does not address the issue of substrate reusability, as residual analytes remain on the substrate. SERS substrates based on photocatalytically active materials can provide reusability for the substrate; however, this feature alone does not fully exploit the potential of the strong SERS enhancement. Combining these techniques into a single experimental protocol promises to create a SERS substrate with even greater advantages. Among the aforementioned techniques, PIERS and photocatalysis share many similarities and exhibit high potential for synergistic integration within a SERS measurement protocol. Mechanistically, a SERS substrate utilizing the PIERS effect is based on a metal/semiconductor nanocomposite structure.[22,24,25] When the semiconductor material is pre-irradiated with UV light, oxygen vacancies can occur on the surface, creating a temporary defect energy level at the metal–semiconductor interface.[22] This leads to an increased charge transfer between the metal and the semiconductor, resulting in a significantly enhanced Raman scattering intensity compared to non-irradiated (*i.e.*, normal SERS) scenarios. Meanwhile, the photocatalytic activity of metal/semiconductor nanocomposite materials is highly regarded and well-documented in numerous studies.[26–28] This structure significantly increases the number of electrons available to participate in reactions, forming hydroxyl radicals (•OH) that decompose organic molecules into water and CO_2 gas.[27,28] Subsequently, the water can be evaporated, and the CO_2 gas diffused into the air, restoring the SERS substrate to a pristine state. Based on this foundation, fabricating a SERS substrate using a metal/semiconductor structure and simultaneously applying both pre- and post-irradiation techniques to combine the synergistic effects of PIERS and photocatalysis in a single SERS protocol can result in several key benefits: (i) high sensitivity due to superior signal enhancement, (ii) substrate reusability contributing to cost-effectiveness and sustainability, and (iii) simplified, scalable experimental procedures suitable for diverse sensing applications. By integrating these mechanisms into a single SERS protocol, this technique not only enhances the overall SERS signal but also offers a practical solution for sustainable and reusable SERS substrates, outperforming conventional techniques in terms of sensitivity, simplicity, and long-term practicality.

Herein, inspired by the PIERS and photocatalysis effects of the metal/semiconductor structure, we introduce a novel technique that combines these two effects on a SERS substrate based on Ag (metal)/TiO_2 (semiconductor) nanocomposite material, termed photo-induced-photo-catalytic SERS (hereafter abbreviated as PI-PC SERS). This approach yields a SERS substrate with simultaneous ultra-sensitive sensing capabilities achieved by pre-irradiating the Ag/TiO_2 substrate with UV light (365 nm) before conducting SERS measurements (PIERS effect), and reusability facilitated by post-irradiation with UV light (365 nm) after SERS measurements (photocatalysis effect). Methylene blue (MB), an organic dye, and thiram, a plant protection agent, were selected as analytes to evaluate the effectiveness of the proposed PI-PC SERS technique. The results demonstrate superior sensor performance of PI-PC SERS compared to normal SERS, with LOD for MB and thiram under PI-PC SERS conditions measured at 1.02×10^{-14} M and 1.02×10^{-11} M, respectively, whereas normal SERS achieves 3.04×10^{-11} M and

2.19×10^{-9} M, respectively. Moreover, the photocatalysis effect was effectively applied to the used Ag/TiO_2 SERS substrate to remove fouled analyte molecules (MB or thiram) from its surface. The decomposition of MB and thiram on the Ag/TiO_2 substrate was evaluated by monitoring the SERS intensity of these molecules over increasing durations of UV irradiation at 365 nm. The results show complete degradation of MB and thiram residues on the Ag/TiO_2 substrate within 60 to 70 minutes of UV irradiation, evidenced by the disappearance of their Raman scattering peaks in the SERS spectra. This process results in a completely refreshed Ag/TiO_2 substrate ready for subsequent PI-PC SERS experiments. Clearly, the PI-PC SERS technique not only improves detection sensitivity and substrate longevity but also offers a sustainable and cost-effective solution for high-performance chemical and bio-analytical sensing applications. This advancement represents a significant step forward in enhancing both the practicality and efficiency of SERS technologies.

2. Methods

2.1. Materials

We obtained precursors from Shanghai Chemical Reagent Co., which included silver nitrate ($AgNO_3$, ≥99.0%), sodium borohydride ($NaBH_4$, 99%), titanium tetrachloride ($TiCl_4$, ≥99.8%), ammonium hydroxide (NH_4OH, 28.0–30.0% NH_3), and ethanol (C_2H_5OH, 98%). Analytes, also sourced from Shanghai Chemical Reagent Co., were methylene blue ($C_{16}H_{18}ClN_3S$, ≥97.0%) and thiram ($C_6H_{12}N_2S_4$, 97.0%). All chemicals were used as received, and double distilled water was utilized throughout the experiments.

2.2. Synthesis and characterizations of Ag/TiO_2 nanocomposite

The Ag/TiO_2 nanocomposite was fabricated following procedures and directly utilized from our previous research.[29] TiO_2 nanoparticles were prepared initially using a modified sol–gel method from $TiCl_4$ precursors. TiO_2 was then thermally treated at 400 °C for 4 hours to ensure total crystallization. Subsequently, Ag nanoparticles were generated by reducing $AgNO_3$ with $NaBH_4$ in the presence of TiO_2 nanoparticles to ensure intimate contact between them. Specifically, 50 mg of TiO_2 powder was dispersed in 50 mL of ethanol (C_2H_5OH) using ultrasonic agitation and mechanical stirring. Next, a specified amount of $AgNO_3$, dissolved in 25 mL of C_2H_5OH, was added to the TiO_2 suspension and stirred for 1 hour to facilitate the interaction between Ag^+ ions and TiO_2. To form Ag nanoparticles, $NaBH_4$, also dispersed in ethanol, was gradually introduced to the solution over a 2 hour period, reducing Ag^+ ions to Ag. The resulting mixture was then filtered, washed three times with C_2H_5OH, and dried at 60 °C to yield the Ag/TiO_2 nanocomposite powder. The ratio of Ag to TiO_2 in the study was chosen as 1 : 1, as it has been shown to provide optimal sensing performance. The morphology of the Ag–TiO_2 nanocomposites was examined using scanning electron microscopy (SEM) with a Hitachi S-4800 instrument, operating at an acceleration voltage of 5 kV. The crystal property of the Ag–TiO_2 nanocomposite was assessed using X-ray diffraction (XRD) with a Bruker D5005 diffractometer, employing Cu Kα radiation ($\lambda = 1.5406$ Å) at 40 kV and 30 mA. Raman spectroscopy (Horiba Macro-RAM™) with a 785 nm laser was utilized to investigate the molecular vibrations and structural properties of the Ag–TiO_2. Additionally, photoluminescence (PL) spectroscopy with a 380 nm excitation wavelength was used to explore the optical properties of the nanocomposite. Results indicated that Ag nanoparticles were formed with an average size of 43 nm and distributed around TiO_2 nanoparticles with an average size of 125 nm. XRD, Raman, and PL measurements confirmed the close interaction between Ag and TiO_2. Detailed characteristics of the Ag/TiO_2 nanocomposite are presented in our previous study.[29]

2.3. SERS measurements

Aluminum (Al) substrates measuring 1 × 1 × 0.1 cm were prepared, featuring a surface-active area with a diameter of 0.2 cm. The substrates were cleaned with ethanol and air-dried at room temperature (RT). A solution of SERS-active substrate was drop-cast onto the surface-active area and dried at RT. Analyte solutions of varying concentrations of MB (10^{-4} M to 10^{-14} M) and thiram (10^{-4} M to 10^{-11} M) were prepared in double-distilled water. Thiram has limited solubility in water, making it challenging to prepare a 10^{-4} M solution using only double-distilled water. To address this, 0.5 mL of ethanol was added as a co-solvent to dissolve appropriate amount of thiram, followed by the addition of 9.5 mL of double-distilled water. Since both solvents were evaporated during the SERS measurements, this did not affect the SERS signals. For each SERS measurement, the sample preparation protocol involved depositing 5 μL of analyte solution directly onto the prepared substrate, followed by natural drying at RT. SERS spectra were acquired using a MacroRaman™ Raman spectrometer (Horiba) equipped with a 785 nm laser excitation. Measurements were conducted with a 100× objective having a numerical aperture of 0.90. The laser power was set at 45 mW, with a 30° incident angle, yielding a diffraction-limited laser spot diameter of 1.1 μm (1.22λ/NA) and a focal length of 115 nm. Each measurement utilized an exposure time of 20 seconds with one accumulation. The intensity of the peaks was determined by considering both the baseline signal caused by fluorescence and the contributions from the Ag/TiO_2 substrate. The fluorescence baseline was subtracted during the measurement, and the contributions from the Ag/TiO_2 substrate were calculated and incorporated into the determination of the analyte's characteristic peak intensity to minimize the impact of overlapping signals and enhance the accuracy of peak intensity determination.

2.4. PIERS experiments and SERS measurements

The PIERS effect was applied in this study following the procedure outlined in Scheme 1. First, Ag/TiO_2 nanocomposites were deposited onto a surface area with a diameter of 0.2 cm and air-dried at room temperature. Subsequently, the Ag/TiO_2 SERS substrate was subjected to pre-irradiation with UV light at

a wavelength of 365 nm (the light source chosen based on prior research to activate the PIERS effect) for 30 minutes (this duration was optimized in our previous study).[29] Immediately thereafter, the analyte MB (or thiram) was applied onto the pre-treated Ag/TiO_2 substrate, and SERS measurements were promptly conducted to mitigate reactivity from the adsorption of environmental oxygen atoms onto the TiO_2 material. The above experimental conditions for the PIERS effect in this study were optimized based on our previous study.[29] The SERS measurements were carried out using the method described above.

2.5. Photocatalysis experiments and SERS measurements

After performing SERS measurements on the Ag/TiO_2 substrate, 5 μL of water was dropped onto the surface to initiate photocatalytic activity. UV irradiation at 365 nm was applied to activate the photocatalytic effect of the Ag/TiO_2 structure. During post-irradiation, SERS measurements were conducted continuously at time intervals of 5, 10, 20, 30… minutes to monitor the photocatalytic efficacy by observing the intensity of characteristic Raman peaks of the analyte. UV irradiation was ceased when the SERS spectrum no longer showed the presence of characteristic Raman peaks of the analyte. At this point, a renewed Ag/TiO_2 substrate was obtained as the analyte-fouled molecules on the surface of the Ag/TiO_2 nanocomposite were completely decomposed into water and CO_2 gas (Scheme 2).

2.6. PI-PC SERS technique experiments

Scheme 3 outlines the protocol for implementing the PI-PC SERS technique on the Ag/TiO_2 SERS substrate in four distinct steps. Step 1 involves preparing the Ag/TiO_2 SERS substrate as detailed previously. Step 2 encompasses the pre-irradiation process. Step 3 entails conducting SERS measurements to capture signal intensities. Step 4 involves post-irradiating the Ag/TiO_2 substrate to degrade residual analytes. This method achieves two pivotal objectives: (i) obtaining robust SERS spectra (greater than the normal SERS signal) of the target analytes, and (ii) obtaining a renewable Ag/TiO_2 SERS substrate for subsequent analyses.

3. Results and discussion

3.1. Efficacy of PI-PC SERS technique on MB analyte

The PI-PC SERS technique involves three stages of light irradiation: (i) stage 1: pre-irradiation of the Ag/TiO_2 substrate with 365 nm UV light to activate the PIERS effect for enhancing the SERS signal; (ii) stage 2: using a 785 nm laser source to capture the SERS signal; (iii) stage 3: post-irradiation with 365 nm UV light to activate the photocatalytic effect for analyte degradation. Initially, the effectiveness of applying the PIERS effect is evaluated by comparing the detection performance of the MB analyte between pre-irradiation and non-pre-irradiation cases.

Fig. 1 illustrates the results of MB detection under normal SERS conditions (*i.e.*, without pre-irradiation) on the Ag/TiO_2 substrate. SERS spectra of MB were acquired across concentrations ranging from 10^{-4} M to 10^{-11} M (Fig. 1a). Characteristic peaks of MB are detailed in Table S1 and Fig. S1a (ESI†). The signal intensities of these characteristic peaks are notably pronounced at concentrations of 10^{-4}, 10^{-5}, and 10^{-6} M, displaying a diminishing trend with decreasing concentration. These peaks are faintly discernible at a concentration of 10^{-10} M and are absent at 10^{-11} M (cannot be clearly distinguished with noise signals). Based on the relationship between the SERS intensities at each concentration, the LOD values were

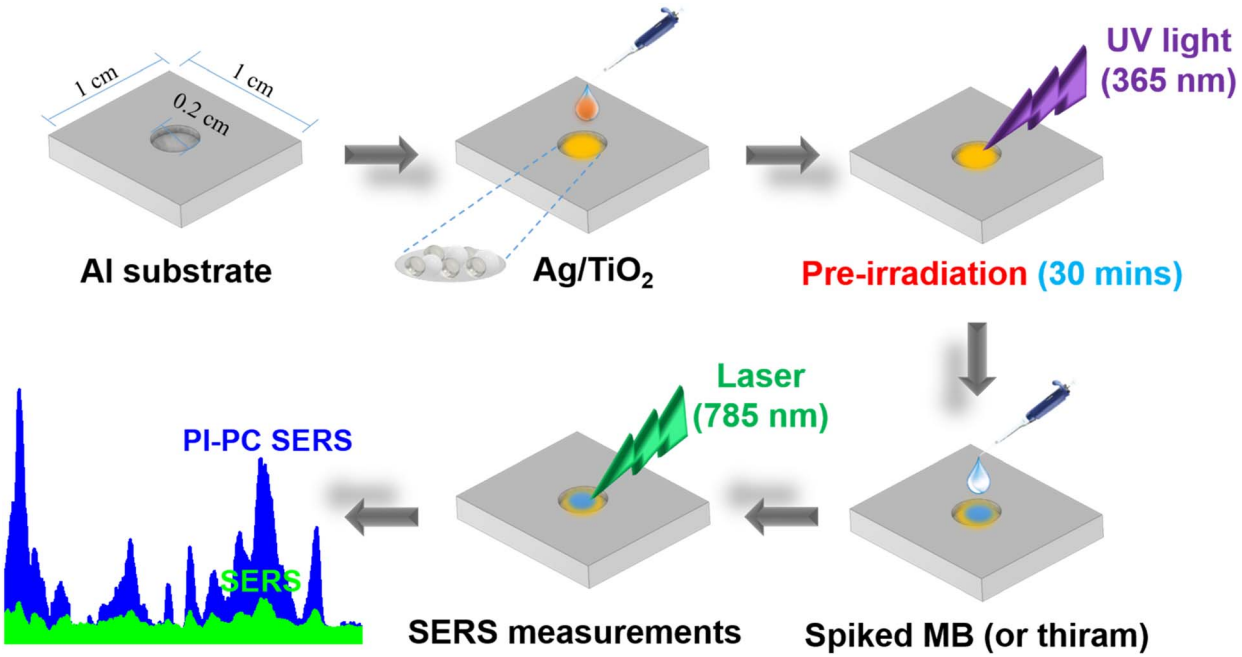

Scheme 1 Pre-irradiation procedure of Ag/TiO_2 SERS substrate in the PI-PC SERS technique for enhancing the SERS signal *via* the PIERS effect.

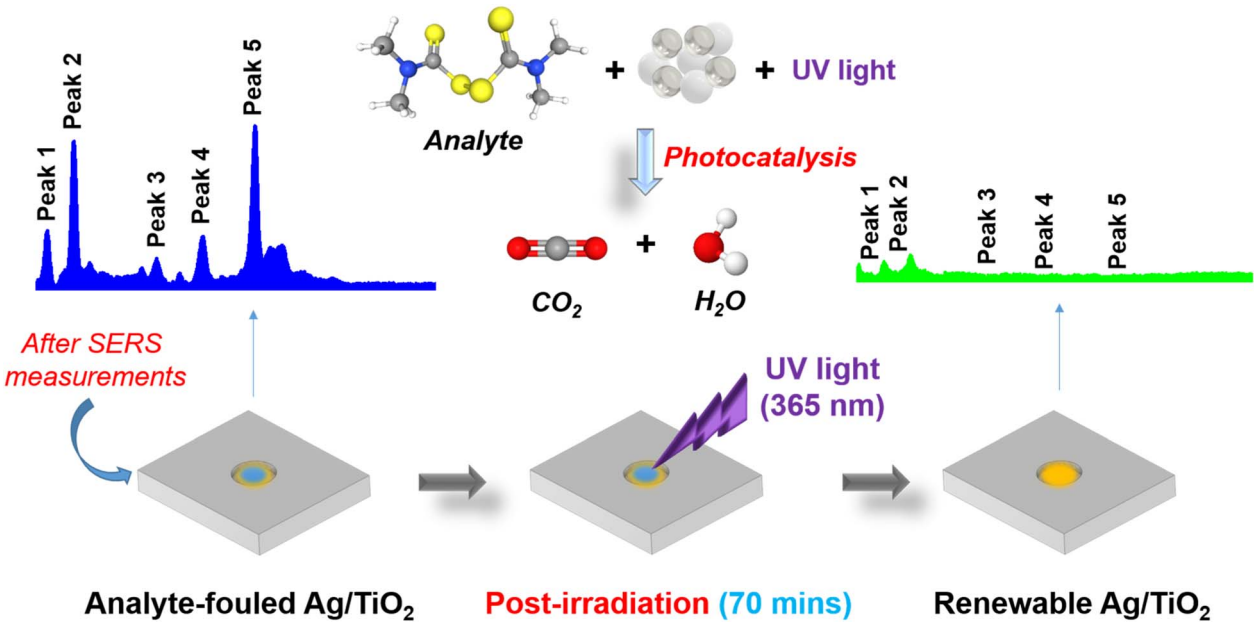

Scheme 2 Post-irradiation process of the Ag/TiO_2 SERS substrate following SERS measurements to utilize photocatalytic effect for obtaining a renewable Ag/TiO_2 substrate.

calculated for the peaks at 460, 1120, 1410, and 1615 cm^{-1}. The linear correlation between the logarithm of the MB concentration and the SERS intensity of the selected peaks is illustrated in Fig. 1b and S1b–d.† The highest linearity was observed at the 460 cm^{-1} peak with an R^2 value of 0.97 over the concentration range of 10^{-7} to 10^{-11} M, while the other peaks exhibited R^2 values < 0.9. SERS spectra of MB at different concentrations in the range of 10^{-7} to 10^{-11} M were also collected to enhance the accuracy of the linear calibration curve (Fig. S2†). The linear calibration curve, established based on 9 data points (Fig. 1b), yields the equation $y = 7.71 + 0.58x$. Using this linear equation and the calculation method detailed in the ESI,† the LOD in this case was determined to be 2.89×10^{-11} M. The practical application of the Ag/TiO_2 substrate was also evaluated over a 60 day storage period and exhibited high long-term stability when stored away from direct exposure to moisture and light (as detailed in Fig. S3 and the ESI†).

Scheme 3 Protocol for implementing the PI-PC SERS technique.

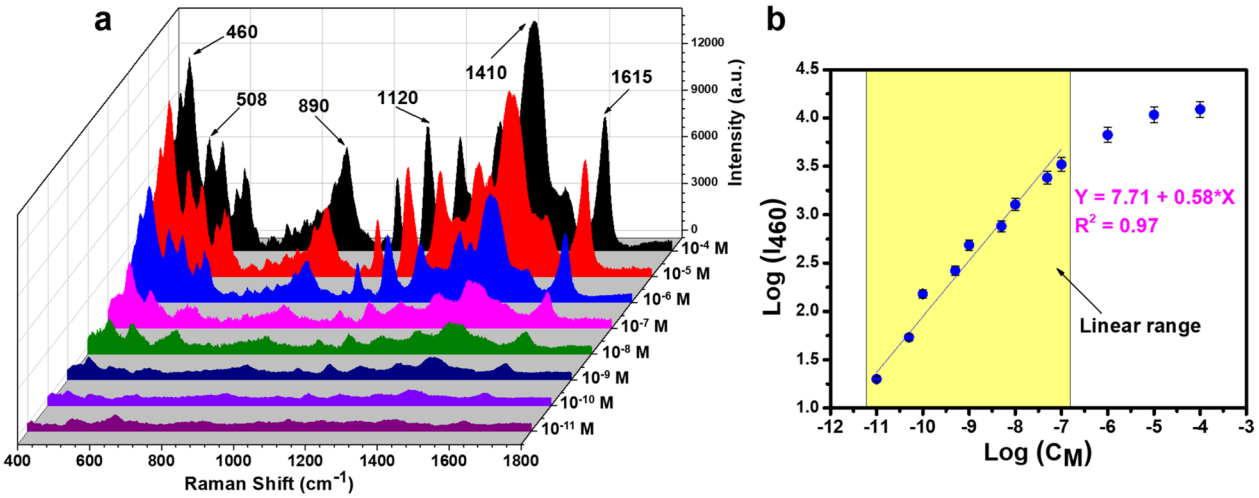

Fig. 1 SERS spectra of MB in the concentration range of 10^{-4} M to 10^{-11} M under normal SERS conditions (a), and the linear relationship between MB concentration and SERS intensity on a logarithmic scale (b).

Applying the PIERS effect in the PI-PC SERS technique is anticipated to significantly enhance the efficiency of MB detection. The experiment involved pre-irradiating the Ag/TiO_2 substrate with 365 nm UV light for 30 minutes prior to depositing the MB analyte and conducting SERS measurements. The results are depicted in Fig. 2 and 3. The SERS peaks at 460, 508, 890, 1120, 1410, and 1615 cm^{-1} remain distinctly visible without any notable shifts, indicating that the pre-irradiation process did not affect the molecular vibrations of MB. Notably, the SERS intensity in the PI-PC SERS approach exhibits significant enhancement compared to normal SERS experiment. Fig. 3a and b compare the SERS signals obtained from PI-PC SERS and normal SERS at MB concentrations of 10^{-6} M and 10^{-10} M, respectively. At the higher concentration of 10^{-6} M, the application of the PIERS technique results in approximately a twofold enhancement in SERS intensity compared to normal SERS, while at the lower concentration of 10^{-10} M, PI-PC SERS demonstrates an impressive 8.8-fold enhancement in SERS signal intensity over normal SERS (comparison of enhancement across the 10^{-4} to 10^{-10} M concentration range at the best linear peak, 460 cm^{-1}, is detailed in Table S2†). This notable enhancement enables the Ag/TiO_2 substrate with PIERS application to detect clear SERS signals from MB molecules even at an ultra-low concentration of 10^{-13} M (see Fig. S4†). Sensitivity metrics were calculated, revealing a linear range from 10^{-9} to 10^{-14} M with a linear equation of $y = 8.70 + 0.55x$ (Fig. 2b), based on 9 data points collected from SERS spectra of closely spaced concentrations to ensure greater accuracy in the linearity within this range (Fig. S5†). The LOD value was determined to be 1.02×10^{-14} M, which represents an improvement of three orders of magnitude over normal SERS. Furthermore, the reliability of the experiment was assessed through parameters

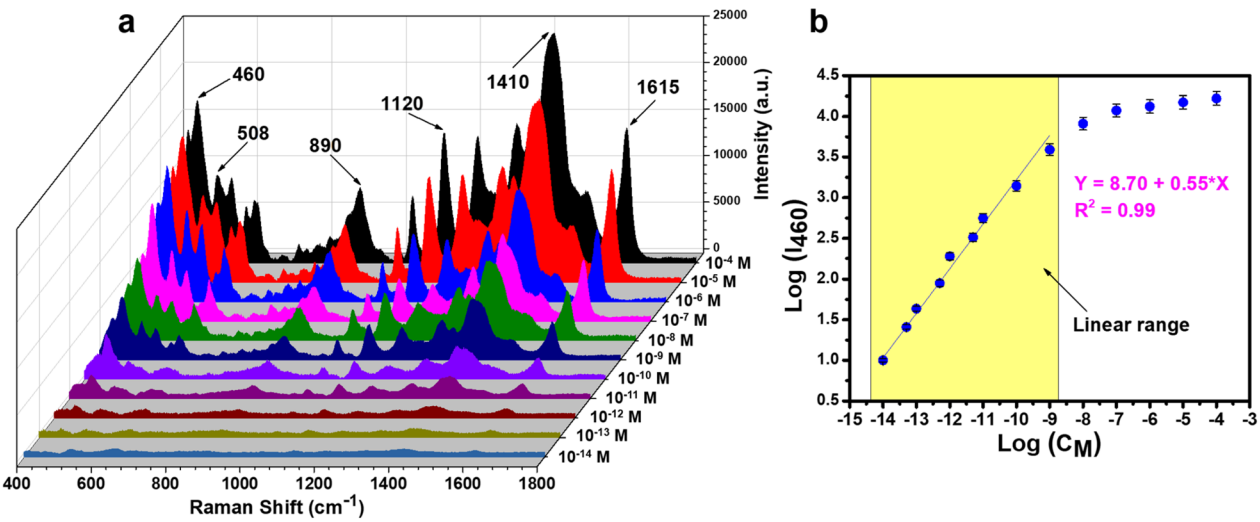

Fig. 2 SERS spectra of MB in the concentration range of 10^{-4} to 10^{-14} M under PI-PC SERS technique (a), and the linear relationship between MB concentration and SERS intensity on a logarithmic scale (b).

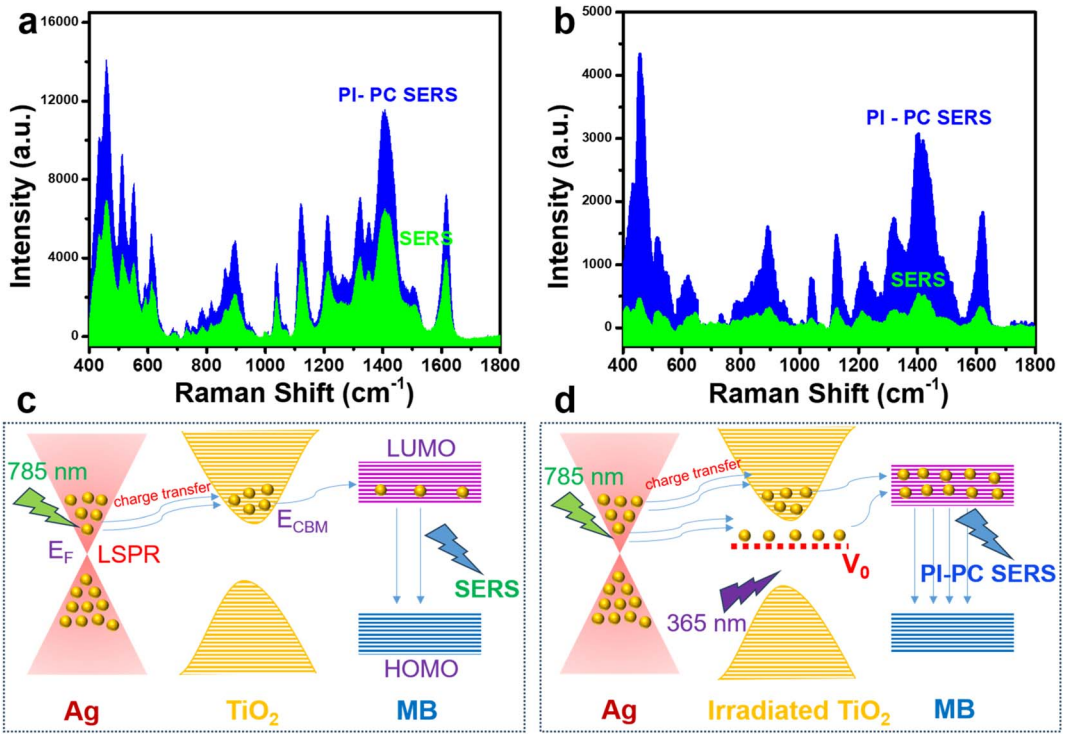

Fig. 3 Comparison of SERS intensity of MB between normal SERS and PI-PC SERS techniques at concentrations of 10^{-6} M (a) and 10^{-10} M (b). Mechanism of normal SERS of the Ag/TiO_2 substrate in MB detection (c) and mechanism of enhanced SERS signal in PI-PC SERS of the Ag/TiO_2 substrate (d).

of repeatability and reproducibility. Repeatability was evaluated by measuring five different points on a single Ag/TiO_2 substrate after irradiation and subsequent analyte addition (Fig. S6a†). Reproducibility was assessed by performing five separate irradiation and SERS signal collection processes on different Ag/TiO_2 substrates (Fig. S6b†). The results demonstrate high experimental reliability, indicated by very low relative standard deviations (RSD) of 5.97% and 6.62% for repeatability and reproducibility, respectively (detailed RSD calculation method in the ESI†). The detection efficiency of MB using the PI-PC SERS technique on the Ag/TiO_2 substrate is significantly superior to the normal SERS technique reported on other SERS substrates. Table 1 compares the MB detection efficiency of normal SERS and PI-PC SERS techniques, highlighting significant improvements in sensitivity, with PI-PC SERS achieving a sensitivity of up to 1.02×10^{-14} M.

The superior enhancement of SERS signals in the PI-PC SERS technique arises from intricate photo-electro interactions within the Ag/TiO_2 transition structure. Fig. 3c and d elucidate the mechanisms in both conventional SERS and PI-PC SERS cases. During SERS measurements, the localized surface plasmon resonance (LSPR) effect in Ag nanoparticles induces charge excitation. These charges are either directly transferred to nearby MB molecules, thereby generating SERS signals, or they interact indirectly *via* TiO_2 intermediates before reaching MB. In normal SERS, excited charges from Ag migrate to the conduction band of TiO_2, which lacks electrons. Subsequently, these charges transition to the lowest unoccupied molecular orbital (LUMO) of MB. Charges returning from the LUMO level to the highest occupied molecular orbital (HOMO) of MB amplify Raman scattering signals. The charge transfer and interactions among light, Ag/TiO_2 nanocomposites, and MB

Table 1 Compare the performance of MB detection using the PI-PC SERS technique with that reported in recent studies (rGO is reduced graphene oxide, GO is graphene oxide)

Substrate	Technique	LOD	Reproducibility	Ref.
Ag–rGO nanocomposite	SERS	1.00×10^{-8} M	—	30
$Ni(OH)_2$/Ag nanocomposites	SERS	1.00×10^{-8} M	—	31
Fe_3O_4/GO/Ag nanocomposite	SERS	1.00×10^{-9} M	—	32
Au/Cu_2O nanocomposite	SERS	3.40×10^{-12} M	<10%	33
Ag/TiO_2 nanocomposite	SERS	2.89×10^{-11} M	—	**This work**
Ag/TiO_2 nanocomposite	PI-PC SERS	1.02×10^{-14} M	6.62%	**This work**

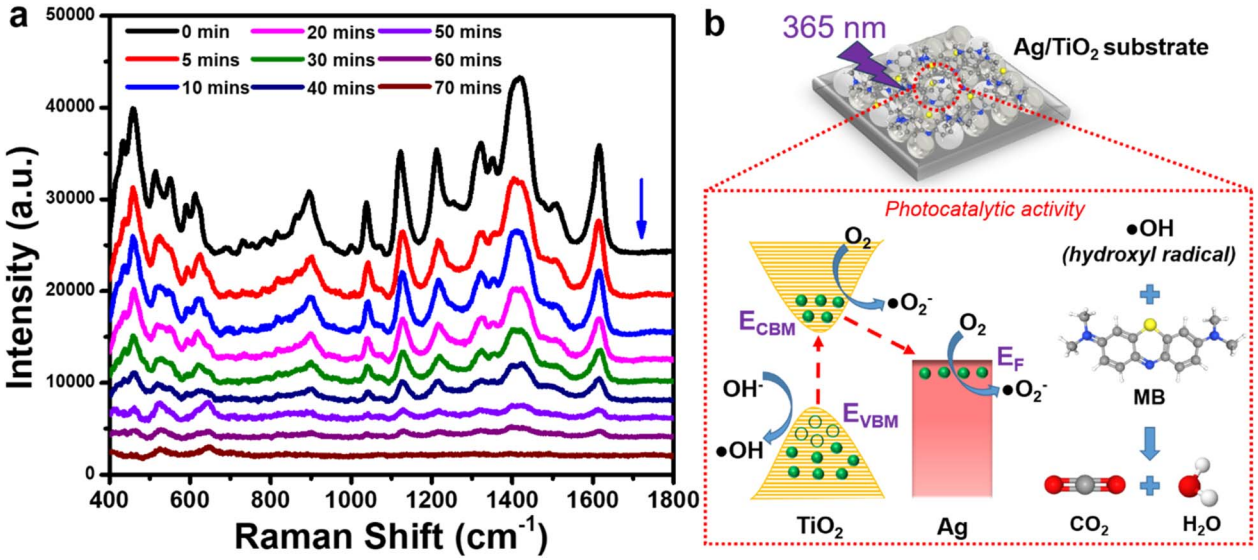

Fig. 4 Photocatalytic activity of the Ag/TiO_2 SERS substrate in MB degradation monitored by SERS spectra (a), and the mechanism of MB degradation by the Ag/TiO_2 nanostructure under UV 365 nm irradiation (b).

molecules significantly enhance SERS signals, enabling detection of MB at near-picogram levels (10^{-11} M). Pre-irradiation of the Ag/TiO_2 structure with 365 nm UV light causes surface oxygen atoms on TiO_2 to eject, forming oxygen vacancies, as previously demonstrated.[22,24,34] Using experimental methods combined with scanning tunneling microscopy, Mezhenny *et al.* provided evidence of defect formation in TiO_2, attributed to the collective removal of oxygen induced by UV light.[35] This process generates a transient intermediate energy state (V_0 in Fig. 3d) within the TiO_2 electronic structure. Henrich *et al.* identified that this V_0 state generates energy levels located approximately 0.7 eV below the minimum conduction band edge of TiO_2.[36] This temporary state facilitates charge transfer from Ag to TiO_2, thereby enhancing the probability and number of charges transferred to surrounding MB molecules near the Ag/TiO_2 nanostructure.[22,37,38] Consequently, this enhancement results in significantly boosted SERS signals compared to normal SERS techniques. However, the ability to maintain the PIERS effect after ceasing the irradiation source needs to be assessed, as oxygen vacancies may be filled by oxygen molecules from the air. This phenomenon of surface healing has been demonstrated by the ability of the TiO_2 surface to adsorb O_2 or H_2O molecules from the air, thereby filling the oxygen vacancies.[39] An experiment evaluating the stability of the PIERS effect on the Ag/TiO_2 substrate was performed by collecting SERS spectra at various time intervals following the pre-irradiation process to further confirm this surface healing phenomenon on the TiO_2 surface. The results are presented in Fig. S7† and the analysis

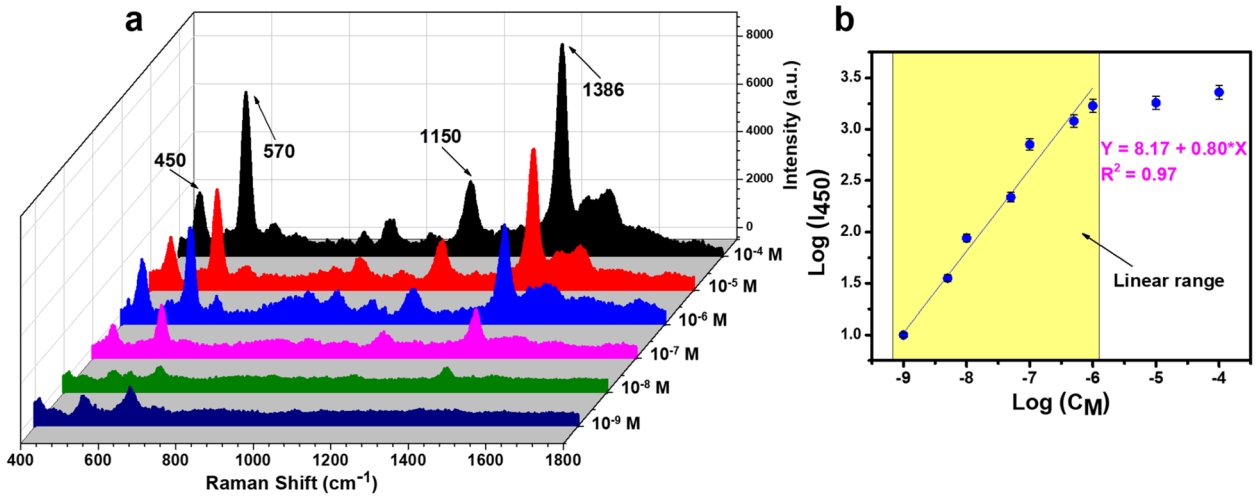

Fig. 5 SERS spectra of thiram in the concentration range of 10^{-4} to 10^{-9} M under normal SERS conditions (a), and the linear relationship between thiram concentration and SERS intensity on a logarithmic scale (b).

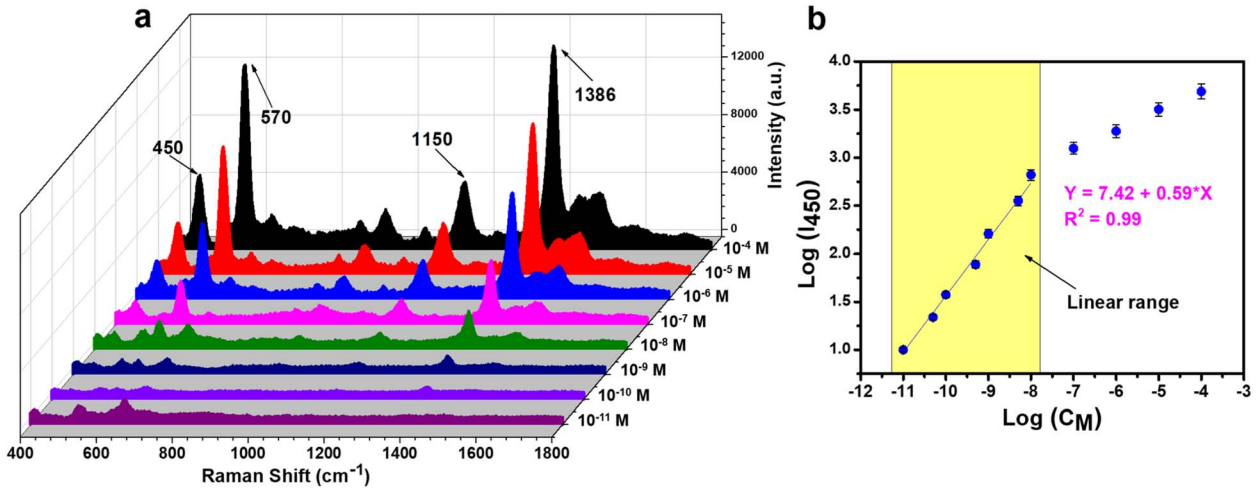

Fig. 6 SERS spectra of thiram in the concentration range of 10^{-4} to 10^{-11} M under PI-PC SERS technique (a), and the linear relationship between thiram concentration and SERS intensity on a logarithmic scale (b).

provided in the ESI† shows that the SERS signal gradually decreased over time as the SERS was exposed to air, which indirectly supports the formation of oxygen vacancies on TiO_2.

In practical terms, once SERS signals have been collected, the SERS substrates are typically rendered unusable due to the accumulation of analyte molecules on their surfaces. Removing these analytes through conventional methods such as washing or thermal decomposition is nearly impractical due to their molecular-level adhesion, which directly affects the substrate's quality. Therefore, reusing SERS substrates to achieve goals such as cost reduction and sustainability poses significant challenges. Apart from successfully exploiting the PIERS effect in Ag/TiO_2 nanostructures as demonstrated earlier, the photocatalytic activity of this structure can be further utilized to

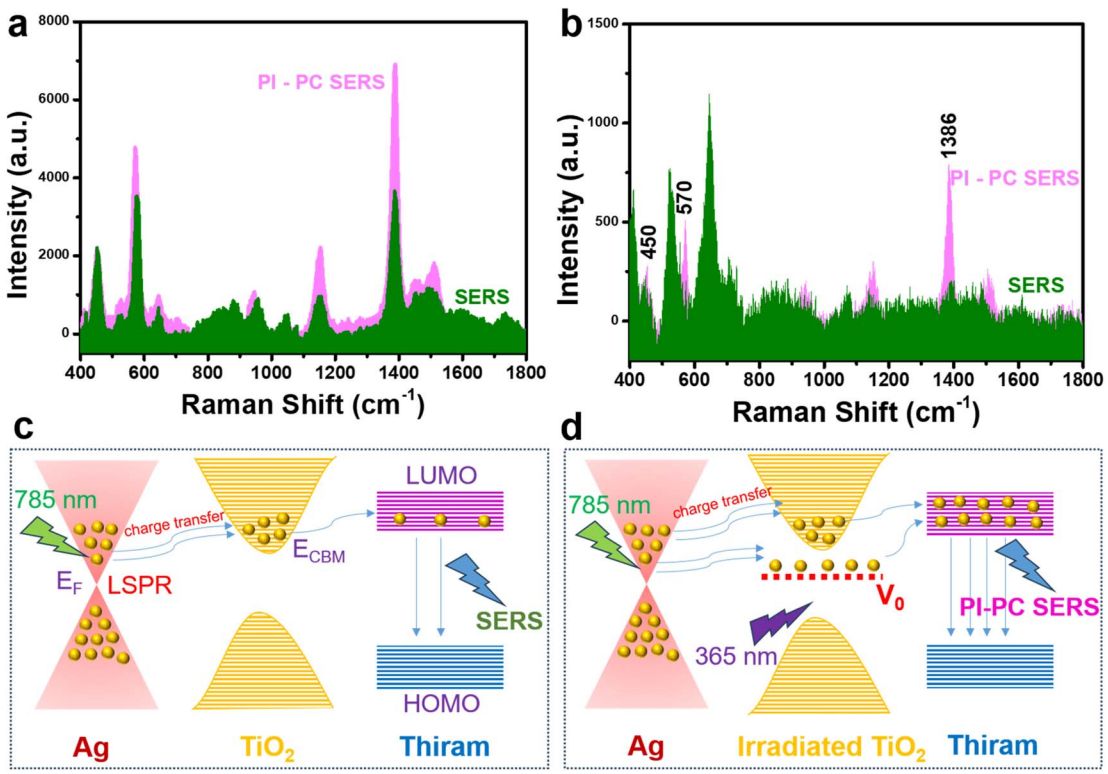

Fig. 7 Comparison of SERS intensity of thiram between normal SERS and PI-PC SERS techniques at concentrations of 10^{-6} M (a) and 10^{-9} M (b). Mechanism of normal SERS of the Ag/TiO_2 substrate in thiram detection (c) and mechanism of enhanced SERS signal in PI-PC SERS of the Ag/TiO_2 substrate (d).

Table 2 Compare the performance of thiram detection using the PI-PC SERS technique with that reported in recent studies (ZIF-67 is zeolitic imidazolate framework-67, Fe_3O_4 is iron(II,III) oxide, MXene is titanium carbide (Ti_3C_2) with surface functional groups, AgNs is Ag nanostars, MoS_2 is molybdenum disulfide, Ag-NP is Ag nanoparticle)

Substrate	Technique	LOD	Reproducibility	Ref.
Ag@ZIF-67 nanocomposite	SERS	1.00×10^{-8} M	—	42
Fe_3O_4@Au nanocomposites	SERS	7.69×10^{-9} M	—	43
MXene/AgNs nanocomposite	SERS	1.00×10^{-8} M	2.22%	44
MoS_2-NS@Ag-NP nanocomposite	SERS	4.20×10^{-8} M		45
Ag/TiO_2 nanocomposite	SERS	2.06×10^{-9} M	—	**This work**
Ag/TiO_2 nanocomposite	PI-PC SERS	1.24×10^{-11} M	7.58%	**This work**

provide additional advantages for SERS substrates based on Ag/TiO_2. If applying pre-UV irradiation at 365 nm has already shown effective improvements in the sensing performance for detecting MB, subsequent UV irradiation at 365 nm could enable self-regeneration of Ag/TiO_2 substrates through photocatalytic activity (details described in the Methods section). The Ag/TiO_2 SERS substrate, after SERS signal collection, is moistened with water and then subjected to UV irradiation at 365 nm (UV region capable of activating TiO_2 photocatalytic effects). SERS signals from this irradiated substrate are continuously recorded at different time intervals during the post-irradiation period, as shown in Fig. 4a. At time point 0 minutes, the SERS signal of MB at a concentration of 10^{-5} M before irradiation is depicted. Subsequent time points (5, 10, 20 minutes, *etc.*) show the SERS results of MB after irradiation. It is evident that the intensity of MB's characteristic peaks decreases gradually over the irradiation period, indicating molecular degradation of MB and consequent weakening of molecular bonds. After just 70 minutes of irradiation, MB's characteristic peaks have completely disappeared (as further observed in Fig. S8†), indicating that MB has been degraded to a level where it no longer interferes with the SERS signal on the Ag/TiO_2 substrate. Fig. 4b succinctly describes the photocatalytic mechanism of MB degradation on Ag/TiO_2 following UV irradiation at 365 nm. Electrons excited by the appropriate wavelength in TiO_2 nanomaterial generate electron–hole pairs, which can react with water and environmental oxygen to produce hydroxyl radicals ($^{\bullet}OH$).[40] These radicals possess the capability to directly oxidize MB molecules, breaking them down into the primary products of water and CO_2.[40,41] This explains why the SERS spectra obtained during photocatalysis do not exhibit additional scattering peaks, as CO_2 can readily diffuse away from the substrate surface, and water molecules do not contribute to Raman signals. Although the MB molecule contains nitrogen (N), sulfur (S), and chlorine (Cl), the degradation products may include these elements, but they are present as monatomic or simple molecular forms. This also does not interfere with the overall SERS spectrum. The presence of Ag nanoparticles enhances the photocatalytic efficiency for MB degradation by facilitating electron transfer between TiO_2 and Ag, thereby minimizing electron–hole recombination and maximizing the number of active electron–hole pairs involved in the reaction. These synergistic interactions within the Ag/TiO_2 composite accelerate MB degradation on the SERS substrate, achieving significant

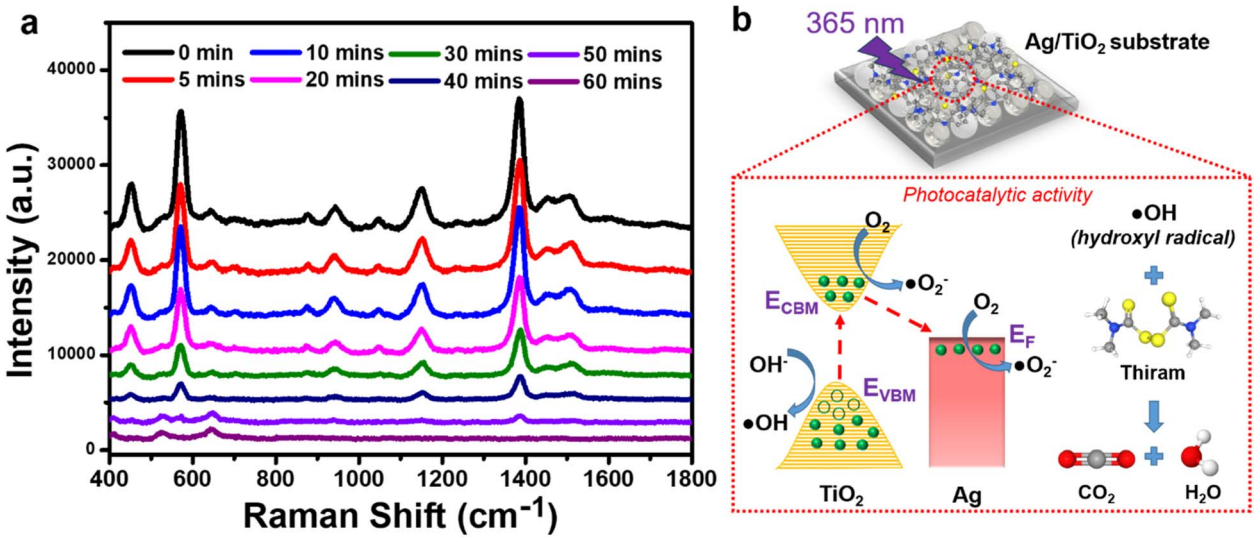

Fig. 8 Photocatalytic activity of the Ag/TiO_2 SERS substrate in thiram degradation monitored by SERS spectra (a), and the mechanism of thiram degradation by the Ag/TiO_2 nanostructure under UV 365 nm irradiation (b).

decomposition within a mere 70 minutes of irradiation. Ultimately, this process yields a fully regenerated Ag/TiO_2 SERS substrate, preserving the original characteristics necessary for subsequent SERS experiments. We term this advantage as renewable ability.

After surface cleaning *via* the photocatalytic effect, the renewable ability of the Ag/TiO_2 substrate was evaluated through its cyclability using the PI-PC SERS technique. This was tested by detecting MB at a concentration of 10^{-6} M over five cycles, following the PI-PC SERS protocol detailed in section 2.5. The byproducts of the photocatalytic process, such as water and CO_2, could potentially interfere with the reusability of the Ag/TiO_2 substrate. Therefore, after the photocatalytic degradation of MB, the Ag/TiO_2 substrate was treated at a temperature of 40 °C for 2 hours to evaporate water and CO_2 generated during the self-cleaning process. The results are presented in Fig. S9.† The data show that the SERS signals obtained from MB across the different cycles are consistent and comparable to those from the initial use (Fig. S9a and b†). This demonstrates that the PI-PC SERS protocol exhibits excellent cyclability, with no significant decline in sensing performance over multiple cycles.

3.2. Efficacy of PI-PC SERS technique on thiram analyte

The renewable Ag/TiO_2 SERS substrate was further assessed for efficacy using the PI-PC SERS technique to establish its reliability. Another experiment applying the PI-PC SERS technique was conducted using a different randomly chosen analyte, thiram pesticide, to evaluate the effectiveness of the PI-PC SERS technique, in addition to the MB analyte. The Ag/TiO_2 substrate, after applying the PI-PC SERS technique to MB, was treated on a heated surface at a temperature of 40 °C for 2 hours to minimize the byproducts of the photocatalytic process. The PI-PC SERS procedure for thiram was conducted similarly to the protocol applied to MB. Initially, the normal SERS signal of thiram on the rejuvenated Ag/TiO_2 substrate was collected for comparison with PI-PC SERS outcomes. The results of thiram detection using normal SERS are illustrated in Fig. 5a. Characteristic peaks of thiram are detailed in Table S3 and Fig. S10a (ESI†). Notably, no interference peaks from MB, the previously used analyte, were observed, indicating the high effectiveness of the rejuvenated Ag/TiO_2 SERS substrate in terms of renewal and reuse. The intensities of the characteristic thiram peaks gradually decreased with decreasing concentration, becoming undetectable at 10^{-9} M. The linear relationship between thiram concentration and SERS intensity was analyzed using a logarithmic function across the four characteristic peaks (Fig. 5b and S10b–d†). SERS spectra of thiram at different concentrations in the range of 10^{-6} to 10^{-9} M were also collected to enhance the accuracy of the linear calibration curve (Fig. S11†). The results revealed that the 450 cm^{-1} peak exhibited the highest linear correlation, with an R^2 value of 0.97 over the linear range from 10^{-6} to 10^{-9} M, described by the equation $y = 8.17 + 0.80x$ based on 7 data points (Fig. 5b). Consequently, the LOD was calculated to be 2.06×10^{-9} M. Thus, despite previous PI-PC SERS experimentation with MB, the renewable Ag/TiO_2 SERS substrate continued to exhibit excellent sensing capabilities for thiram.

The efficacy of normal SERS sensing on the renewable Ag/TiO_2 substrate has been demonstrated to persist for thiram. A critical inquiry arises regarding the sustained efficacy of the PI-PC SERS technique on this substrate. The PI-PC SERS experiment commenced with pre-irradiating the Ag/TiO_2 substrate using 365 nm UV light for 30 minutes, followed by the introduction of the thiram onto the substrate and immediate collection of SERS signals thereafter. The efficacy of thiram detection using PI-PC SERS is illustrated in Fig. 6. The distinctive peaks of thiram are vividly resolved and sharply defined. Notably, the SERS signal intensity obtained surpasses that of normal SERS. At a concentration of 10^{-6} M (Fig. 7a), the SERS signal from PI-PC SERS is 1.75 times higher than that from normal SERS, rising to 8.68 times at 10^{-9} M (Fig. 7b). While the characteristic SERS peaks vanish completely at 10^{-9} M concentration for normal SERS, those at 450, 570, and 1386 cm^{-1} persist at 10^{-10} M concentration for PI-PC SERS. The 450 cm^{-1} peak exhibits an excellent linear correlation between concentration and SERS intensity with an R^2 value of 0.99 (Fig. 6b and S12†). The linear range spans from 10^{-8} M to 10^{-11} M with a linear equation of $y = 7.42 + 0.59x$, and the calculated LOD is 1.24×10^{-11} M, two orders of magnitude superior to that of normal SERS. The reliability of the PI-PC SERS experiment on the Ag/TiO_2 substrate for thiram analysis is further evaluated through parameters of repeatability and reproducibility (Fig. S13a and b†). The results demonstrate high reliability with RSD values for repeatability and reproducibility of 5.68% and 7.58%, respectively.

Table 2 compares the detection efficiency of thiram on various SERS substrates using normal SERS and PI-PC SERS techniques, showing a significant improvement in sensitivity with PI-PC SERS, achieving a LOD of 10^{-11} M. The mechanism underlying the amplified SERS signal of the PI-PC SERS technique relative to normal SERS is elucidated in Fig. 7c and d. The occurrence of oxygen vacancies on the TiO_2 surface induced by UV irradiation generates an intermediate energy level between the valence and conduction bands of TiO_2, thereby enhancing the probability and number of charge transfer from Ag to TiO_2, subsequently to thiram. This cascade effect culminates in higher SERS signals from the PI-PC SERS technique.

The renewable and reusable capabilities of the Ag/TiO_2 SERS substrate were further assessed following sensor signal acquisition with thiram. The photocatalytic outcomes under 365 nm UV irradiation in the presence of water are presented in Fig. 8. It is apparent that the SERS signal from thiram gradually diminishes over the duration of post-irradiation. After 60 minutes of irradiation and photocatalytic activity, the Ag/TiO_2 SERS substrate demonstrates cleanliness as the thiram SERS signal completely vanishes, revealing only the scattering peaks of the Ag/TiO_2 substrate material (Fig. 8a). The photocatalytic degradation mechanism for thiram is elucidated in Fig. 8b, akin to the degradation pathway observed for MB, driven by the formation of $^{\bullet}OH$ radicals proficient in decomposing adjacent organic molecules. The resultant products, water and CO_2 gas, facilitate vaporization, thereby facilitating the regeneration of

a pristine Ag/TiO_2 substrate, primed for reuse in subsequent applications. Thus, the PI-PC SERS technique has been rigorously appraised and has exhibited consistent efficacy in thiram analysis, showcasing both amplified SERS performance *via* the PIERS effect and rejuvenation capacity through photocatalytic mechanisms. The demonstrated feasibility and efficacy across multiple usage cycles underscore the PI-PC SERS technique introduced in this study as highly promising for practical applications.

4. Conclusions

In conclusion, we have demonstrated the PI-PC SERS technique by harnessing the synergistic interplay between PIERS and photocatalysis effects on an Ag/TiO_2 nanocomposite-based SERS substrate. By pre-irradiating the Ag/TiO_2 substrate with 365 nm UV light to activate its PIERS effect, we achieved a substantial enhancement in the SERS signal of the analyte compared to normal SERS, thereby significantly improving sensing performance. Subsequently, efficient photocatalytic decomposition of residual analyte molecules on the Ag/TiO_2 substrate under 365 nm UV light further exemplified its capability to renew and prepare the SERS substrate for other analytical measurements. The high reliability of this introduced PI-PC SERS technique was proved through consistent experimental protocols applied to two distinct analytes, MB and thiram. Our findings underscore the robust preservation of both PIERS and photocatalytic functionalities across multiple reuse cycles, affirming the sustained efficacy of the PI-PC SERS approach. This innovative integration of cooperative PIERS and photocatalysis within the PI-PC SERS technique presents a compelling strategy for designing sensing approach that offer superior sensitivity while ensuring recyclability, aligning seamlessly with contemporary imperatives for sustainable technological development. This study paves the way for further exploration of PI-PC SERS methodologies across other nanocomposite materials and diverse analytes, promising new frontiers in analytical techniques and sensor design.

Data availability

The data that support the findings of this study are available from the corresponding author upon reasonable request. All experimental results, including those for SERS and PIERS sensing detection and the photocatalysis of methylene blue dye and thiram pesticide, are provided within the manuscript and its supplementary information.†

Author contributions

Q. D. Mai: conceptualization, methodology, investigation, formal analysis, writing-original draft; D. T. H. Trang: validation, investigation; T. N. Bach: validation, Investigation; V. L. Na: validation, investigation; A. T. Pham: methodology, formal analysis, supervision; A. T. Le: conceptualization, methodology, supervision, project administration, writing-review & editing.

Conflicts of interest

The authors declare that they have no known competing financial interests or personal relationships that could have appeared to influence the work reported in this paper.

Acknowledgements

This research was acknowledged to the Phenikaa University under grant number PU2023-2-A-03 & A&A Green Phoenix Group JSC through Financial Supports for Purchasing Research Equipments of Key Research Group (NEB Lab). The authors would like to acknowledge the supports for Raman & SERS measurements from NEB Lab (Phenikaa University).

References

1 S.-Y. Ding, J. Yi, J.-F. Li, B. Ren, D.-Y. Wu, R. Panneerselvam, *et al.*, Nanostructure-based plasmon-enhanced Raman spectroscopy for surface analysis of materials, *Nat. Rev. Mater.*, 2016, **1**(6), 1–16.
2 X. X. Han, R. S. Rodriguez, C. L. Haynes, Y. Ozaki and B. Zhao, Surface-enhanced Raman spectroscopy, *Nat. Rev. Methods Primers*, 2021, **1**(1), 87.
3 S. Nie and S. R. Emory, Probing single molecules and single nanoparticles by surface-enhanced Raman scattering, *Science*, 1997, **275**(5303), 1102–1106.
4 S. Zeng, D. Baillargeat, H.-P. Ho and K.-T. Yong, Nanomaterials enhanced surface plasmon resonance for biological and chemical sensing applications, *Chem. Soc. Rev.*, 2014, **43**(10), 3426–3452.
5 J. F. Betz, W. Y. Wei, Y. Cheng, I. M. White and G. W. Rubloff, Simple SERS substrates: powerful, portable, and full of potential, *Phys. Chem. Chem. Phys.*, 2014, **16**(6), 2224–2239.
6 B. Sharma, R. R. Frontiera, A.-I. Henry, E. Ringe and R. P. Van Duyne, SERS: materials, applications, and the future, *Mater. Today*, 2012, **15**(1–2), 16–25.
7 J. Langer, D. Jimenez de Aberasturi, J. Aizpurua, R. A. Alvarez-Puebla, B. Auguié, J. J. Baumberg, *et al.*, Present and future of surface-enhanced Raman scattering, *ACS Nano*, 2019, **14**(1), 28–117.
8 O. Siiman, L. Bumm, R. Callaghan, C. Blatchford and M. Kerker, Surface-enhanced Raman scattering by citrate on colloidal silver, *J. Phys. Chem.*, 1983, **87**(6), 1014–1023.
9 S. E. Bell and M. R. McCourt, SERS enhancement by aggregated Au colloids: effect of particle size, *Phys. Chem. Chem. Phys.*, 2009, **11**(34), 7455–7462.
10 R. G. Freeman, K. C. Grabar, K. J. Allison, R. M. Bright, J. A. Davis, A. P. Guthrie, *et al.*, Self-assembled metal colloid monolayers: an approach to SERS substrates, *Science*, 1995, **267**(5204), 1629–1632.
11 M. J. Banholzer, J. E. Millstone, L. Qin and C. A. Mirkin, Rationally designed nanostructures for surface-enhanced Raman spectroscopy, *Chem. Soc. Rev.*, 2008, **37**(5), 885–897.
12 S. Fateixa, H. I. Nogueira and T. Trindade, Hybrid nanostructures for SERS: materials development and

chemical detection, *Phys. Chem. Chem. Phys.*, 2015, **17**(33), 21046–21071.

13 K. L. Lee, C. Y. Hung, M. Y. Pan, T. Y. Wu, S. Y. Yang and P. K. Wei, Dual Sensing Arrays for Surface Plasmon Resonance (SPR) and Surface-Enhanced Raman Scattering (SERS) Based on Nanowire/Nanorod Hybrid Nanostructures, *Adv. Mater. Interfaces*, 2018, **5**(21), 1801064.

14 T. Wang, S. Wang, Z. Cheng, J. Wei, L. Yang, Z. Zhong, *et al.*, Emerging core–shell nanostructures for surface-enhanced Raman scattering (SERS) detection of pesticide residues, *Chem. Eng. J.*, 2021, **424**, 130323.

15 J. F. Li, Y. F. Huang, Y. Ding, Z. L. Yang, S. B. Li, X. S. Zhou, *et al.*, Shell-isolated nanoparticle-enhanced Raman spectroscopy, *Nature*, 2010, **464**(7287), 392–395.

16 Q.-D. Mai, D. C. Thanh, N. T. Anh, T. Van Manh, T. N. Bach, H.-A. Nguyen, *et al.*, Smart 3D Ag-decorated TiO2 nanostructure: an advanced synergistic SERS substrate for trace detection of analytes with diverse natures, *Sens. Actuators, B*, 2024, **410**, 135651.

17 H. K. Lee, Y. H. Lee, C. S. L. Koh, G. C. Phan-Quang, X. Han, C. L. Lay, *et al.*, Designing surface-enhanced Raman scattering (SERS) platforms beyond hotspot engineering: emerging opportunities in analyte manipulations and hybrid materials, *Chem. Soc. Rev.*, 2019, **48**(3), 731–756.

18 M. F. Cardinal, E. Vander Ende, R. A. Hackler, M. O. McAnally, P. C. Stair, G. C. Schatz, *et al.*, Expanding applications of SERS through versatile nanomaterials engineering, *Chem. Soc. Rev.*, 2017, **46**(13), 3886–3903.

19 T. Itoh, M. Procházka, Z.-C. Dong, W. Ji, Y. S. Yamamoto, Y. Zhang, *et al.*, Toward a new era of SERS and TERS at the nanometer scale: from fundamentals to innovative applications, *Chem. Rev.*, 2023, **123**(4), 1552–1634.

20 G. G. Huang, X. X. Han, M. K. Hossain and Y. Ozaki, Development of a heat-induced surface-enhanced Raman scattering sensing method for rapid detection of glutathione in aqueous solutions, *Anal. Chem.*, 2009, **81**(14), 5881–5888.

21 S. Almohammed, F. Zhang, B. J. Rodriguez and J. H. Rice, Electric field-induced chemical surface-enhanced Raman spectroscopy enhancement from aligned peptide nanotube–graphene oxide templates for universal trace detection of biomolecules, *J. Phys. Chem. Lett.*, 2019, **10**(8), 1878–1887.

22 S. Ben-Jaber, W. J. Peveler, R. Quesada-Cabrera, E. Cortés, C. Sotelo-Vazquez, N. Abdul-Karim, *et al.*, Photo-induced enhanced Raman spectroscopy for universal ultra-trace detection of explosives, pollutants and biomolecules, *Nat. Commun.*, 2016, **7**(1), 12189.

23 T. Wu, H. Zheng, Y. Kou, X. Su, N. R. Kadasala, M. Gao, *et al.*, Self-sustainable and recyclable ternary Au@ Cu2O–Ag nanocomposites: application in ultrasensitive SERS detection and highly efficient photocatalysis of organic dyes under visible light, *Microsyst. Nanoeng.*, 2021, **7**(1), 23.

24 J. Ye, R. Arul, M. K. Nieuwoudt, J. Dong, T. Zhang, L. Dai, *et al.*, Understanding the chemical mechanism behind photoinduced enhanced raman spectroscopy, *J. Phys. Chem. Lett.*, 2023, **14**(19), 4607–4616.

25 K. Abid, N. H. Belkhir, S. B. Jaber, R. Zribi, M. G. Donato, G. Di Marco, *et al.*, Photoinduced enhanced raman spectroscopy with hybrid Au@ WS2 nanosheets, *J. Phys. Chem. C*, 2020, **124**(37), 20350–20358.

26 F. Petronella, E. Fanizza, G. Mascolo, V. Locaputo, L. Bertinetti, G. Martra, *et al.*, Photocatalytic activity of nanocomposite catalyst films based on nanocrystalline metal/semiconductors, *J. Phys. Chem. C*, 2011, **115**(24), 12033–12040.

27 P. Zhou, M. Luo and S. Guo, Optimizing the semiconductor–metal-single-atom interaction for photocatalytic reactivity, *Nat. Rev. Chem*, 2022, **6**(11), 823–838.

28 K. Maeda, Metal-complex/semiconductor hybrid photocatalysts and photoelectrodes for CO_2 reduction driven by visible light, *Adv. Mater.*, 2019, **31**(25), 1808205.

29 Q. D. Mai, H. A. Nguyen, T. L. H. Phung, N. Xuan Dinh, Q. H. Tran, T. Q. Doan, *et al.*, Photoinduced Enhanced Raman Spectroscopy for the Ultrasensitive Detection of a Low-Cross-Section Chemical, Urea, Using Silver–Titanium Dioxide Nanostructures, *ACS Appl. Nano Mater.*, 2022, **5**(10), 15518–15530.

30 P. Chettri, V. Vendamani, A. Tripathi, M. K. Singh, A. P. Pathak and A. Tiwari, Green synthesis of silver nanoparticle-reduced graphene oxide using Psidium guajava and its application in SERS for the detection of methylene blue, *Appl. Surf. Sci.*, 2017, **406**, 312–318.

31 X. Wen, H. Cheng, W. Zhang, L. You and J. Li, Multifunctional Ni $(OH)_2$/Ag composites for ultrasensitive SERS detection and efficient photocatalytic degradation of ciprofloxacin and methylene blue, *Talanta*, 2024, **266**, 125140.

32 J. He, G. Song, X. Wang, L. Zhou and J. Li, Multifunctional magnetic Fe_3O_4/GO/Ag composite microspheres for SERS detection and catalytic degradation of methylene blue and ciprofloxacin, *J. Alloys Compd.*, 2022, **893**, 162226.

33 E. A. Kumar, T.-J. Wang and Y.-H. Chang, Ultrasensitive SERS substrates based on Au nanoparticles photo-decorated on Cu_2O microspheres for the detection of rhodamine B and methylene blue, *Appl. Surf. Sci.*, 2022, **585**, 152696.

34 M. P. Le, N. H. Pham, T. H. Y. Le, V. T. Nguyen, T. H. Pham, T. San Nguyen, *et al.*, Unraveling the mechanism of photo-induced surface enhanced Raman scattering on ZnO/Au thin films, *Appl. Surf. Sci.*, 2024, **657**, 159785.

35 S. Mezhenny, P. Maksymovych, T. Thompson, O. Diwald, D. Stahl, S. Walck, *et al.*, STM studies of defect production on the TiO_2 (110)-(1× 1) and TiO_2 (110)-(1× 2) surfaces induced by UV irradiation, *Chem. Phys. Lett.*, 2003, **369**(1–2), 152–158.

36 V. E. Henrich, G. Dresselhaus and H. Zeiger, Observation of Two-Dimensional Phases Associated with Defect States on the Surface of TiO_2, *Phys. Rev. Lett.*, 1976, **36**(22), 1335.

37 K. Iida and M. Noda, Electron transfer governed by light–matter interaction at metal–semiconductor interface, *npj Comput. Mater.*, 2020, **6**(1), 5.

38 Z. Mao, W. Song, L. Chen, W. Ji, X. Xue, W. Ruan, *et al.*, Metal–semiconductor contacts induce the charge-transfer

mechanism of surface-enhanced Raman scattering, *J. Phys. Chem. C*, 2011, **115**(37), 18378–18383.

39 K. Onda, B. Li and H. Petek, Two-photon photoemission spectroscopy of Ti O 2 (110) surfaces modified by defects and O_2 or H_2O adsorbates, *Phys. Rev. B:Condens. Matter Mater. Phys.*, 2004, **70**(4), 045415.

40 S. Gligorovski, R. Strekowski, S. Barbati and D. Vione, Environmental implications of hydroxyl radicals (• OH), *Chem. Rev.*, 2015, **115**(24), 13051–13092.

41 D. Taraborrelli, M. G. Lawrence, J. N. Crowley, T. J. Dillon, S. Gromov, C. B. Groß, *et al.*, Hydroxyl radical buffered by isoprene oxidation over tropical forests, *Nat. Geosci.*, 2012, **5**(3), 190–193.

42 Y. Yuan, L. Gao, Y. Luo, J. Mi, Z. Cao, M. Wang, *et al.*, Ag@ZIF-67 nanocomposites for ultra-sensitive SERS detection to thiram molecules, *J. Phys. D: Appl. Phys.*, 2023, **56**(5), 055302.

43 D. Han, B. Li, Y. Chen, T. Wu, Y. Kou, X. Xue, *et al.*, Facile synthesis of Fe_3O_4@ Au core–shell nanocomposite as a recyclable magnetic surface enhanced Raman scattering substrate for thiram detection, *Nanotechnology*, 2019, **30**(46), 465703.

44 N. N. Yusoff, F. S. Nor Azmi, B. N. Abu, T. H. Tengku Abdul Aziz and J. G. Shapter, Titanium carbide MXene/silver nanostars composite as SERS substrate for thiram pesticide detection, *Chem. Pap.*, 2024, **78**(5), 2855–2865.

45 X. Liang, Y.-S. Wang, T.-T. You, X.-J. Zhang, N. Yang, G.-S. Wang, *et al.*, Interfacial synthesis of a three-dimensional hierarchical MoS_2-NS@ Ag-NP nanocomposite as a SERS nanosensor for ultrasensitive thiram detection, *Nanoscale*, 2017, **9**(25), 8879–8888.